RESEARCH ARTICLE

NANO · MICRO small
www.small-journal.com

Mechanocatalytic Synthesis of Ammonia by Titanium Dioxide with Bridge-Oxygen Vacancies: Investigating Mechanism from the Experimental and First-Principle Approach

Chengli He, Yang Chen, Zixiang Hao, Linrui Wang, Mingyan Wang, and Xiaoli Cui**

Mechanochemical ammonia (NH_3) synthesis is an emerging mild approach derived from nitrogen (N_2) gas and hydrogen (H) source. The gas-liquid phase mechanochemical process utilizes water (H_2O), rather than conventional hydrogen (H_2) gas, as H sources, thus avoiding carbon dioxide (CO_2) emission during H_2 production. However, ammonia yield is relatively low to meet practical demand due to huge energy barriers of N_2 activation and H_2O dissociation. Here, six transition metal oxides (TMO) such as titanium dioxide (TiO_2), iron(III) oxide (Fe_2O_3), copper(II) oxide (CuO), niobium(V) oxide(Nb_2O_5), zinc oxide (ZnO), and copper(I) oxide (Cu_2O) are investigated as catalysts in mechanochemical N_2 fixation. Among them, TiO_2 shows the best mechanocatalytic effect and the optimum reaction rate constant is 3.6-fold higher than the TMO-free process. The theoretical calculations show that N_2 molecules prefer to side-on chemisorb on the mechano-induced bridge-oxygen vacancies in the (101) crystal plane of TiO_2 catalyst, while H_2O molecules can dissociate on the same sites more easily to provide free H atoms, enabling an alternative-way hydrogeneration process of activated N_2 molecules to release NH_3 eventually. This work highlights the cost-effective TiO_2 mechanocatalyst for ammonia synthesis under mild conditions and proposes a defect-engineering-induced mechanocatalytic mechanism to promote N_2 activation and H_2O dissociation.

1. Introduction

Ammonia (NH_3) is a key precursor for fertilizers, fibers, plastics, explosives, and other chemicals.[1–3] It is also an ideal hydrogen carrier with a high hydrogen density at 17.6 wt.% and low liquefying pressure ≈8 atm,[4,5] and a promising zero-carbon fuel with a high energy density at 4.3 kW h L^{-1}.[6,7] NH_3 mainly derives from geochemical processes,[8] biological photocatalytic N_2 fixation,[9] and the well-known industrially thermos-catalytic Haber–Bosch process.[10] The Haber–Bosch method has hugely promoted the development of the nitrogen fertilizer industry, bringing a nearly 400% increment in crop yield adapting to the rapidly growing global population,[8] and has been awarded the Nobel Prize in chemistry three times.[11] Nevertheless, this process suffers from a relatively low NH_3 single-pass conversion (< 15%), and its critical operation conditions of elevated temperature (400–600 °C) and high pressure (20–40 MPa) account for 1–2% of the annual global energy consumption, and simultaneously producing H_2 feedstocks causes more than 1% of global CO_2 emissions.[6,12,13] Therefore, developing alternative scalable mild-condition ammonia synthesis routes ambient temperature and pressure is desired for efficient, energy-saving, and decarbonized NH_3 production.

Numerous accessible strategies involving photocatalysis,[14–17] electrocatalysis,[18,19] plasma-based catalysis,[20,21] photoelectrochemistry,[22,23] biochemistry,[24] and mechanochemistry[3,11,25] have been explored for NH_3 production. Mechanochemistry, typically realized through ball milling, is an emerging method of initiating or accelerating chemical reactions by mechanical energy obtained by shearing, grinding, stretching, cavitation, and high pressure.[26–29] By creating fresh-reactive surfaces, highly active vacancies, or transient hot spots from the collisions with milling media and catalysts, new reaction routes or unexpected products (e.g., inorganic synthesis,[30–33] organic synthesis,[34–37] gas synthesis,[38,39] and others[40]) can be achieved even under mild conditions.[25] The concept of mechanochemical N_2 fixation to directly synthesize NH_3 was initially raised in 1961.[11,41,42] In 2020, Tricker and co-workers introduced TiN as an effective catalyst to mechanically activate N_2 and H_2 to synthesize NH_3, involving the

C. He, Y. Chen, Z. Hao, L. Wang, X. Cui
Department of Materials Science
Fudan University
Shanghai 200433, P. R. China
E-mail: yangchen@shnu.edu.cn; xiaolicui@fudan.edu.cn
Y. Chen
College of Chemistry and Materials Science
Shanghai Normal University
Shanghai 200234, P. R. China
M. Wang
School of Environment and Chemical Engineering
Jiangsu Ocean University
Lianyungang 222005, P. R. China
The ORCID identification number(s) for the author(s) of this article can be found under https://doi.org/10.1002/smll.202309500

DOI: 10.1002/smll.202309500

incorporation of N_2 into Ti lattice and further hydrogenation of TiN under a transient Mars-van Krevelen mechanism.[25] Then, Han et al. found that NH_3 can be directly produced from N_2 and H_2 via a Fe-catalyzed mechanochemical process at 45 °C and 1 bar and the NH_3 yield reached 45 μmol g_{cat}^{-1} h^{-1}.[3] In 2021, Reichle et al. reported a cesium-promoted iron catalyst, making the mechanochemical N_2 fixation operate at room temperature and 1 bar, and showed an efficient NH_3 yield of more than 0.2 vol% over 50 h.[11] Great efforts have been devoted to reducing energy consumption by lowering the temperature and working pressure, yet hydrogen gas is still chosen as the proton source in these gas-phase mechanochemical processes.

Very recently, we demonstrated a one-pot aqueous mechanochemical ammonia synthesis route by employing N_2 gas and H_2O (liquid) as the feedstocks under room temperature and atmospheric pressure, and the NH_4^+ selectivity is up to 99.2 wt.%.[43] Though the 304-stainless steel ball-milling equipment itself played an vital catalytic role in promoting N_2 activation and H_2O dissociation, we kept exploring more favorable mechanocatalysts to enlarge the NH_3 yield and selectivity in this gas-liquid system. It was reported that the in-situ formed TiN could act as a catalyst for the mechanochemical synthesis of ammonia using N_2 and H_2 as precursors.[25] Also, both theoretical and experimental studies claimed that various transition metal nitrides (MoN_2,[44] Mn_4N,[45] VN,[46] and others[47]) have electrocatalytic N_2 reduction capability under mild conditions. However, Hu et al. found that the NH_3 generation originates from the fast chemical decomposition of tetragonal Mo_2N in aqueous electrolytes rather than direct electrocatalytic N_2 reduction.[48] Thus, transition metal nitrides may not be the most suitable mechanocatalyst candidate in the aqueous mechanochemical N_2 fixation process due to poor chemical stability in presence of liquid feedstock.

Here, we employed several transition metal oxide (TMO) catalysts (TiO_2, CuO, Fe_2O_3, Nb_2O_5, ZnO, and Cu_2O) in this gas-liquid mechanochemical process. The TiO_2 dominated with (101) crystal plane shows the highest positive mechanocatalytic activity and a defect-induced enhancement mechanism is proposed according to DFT calculations. The N_2 molecules prefer to side-on chemisorb on the bridge-O vacancies of the TiO_2(101) surface, while H_2O molecules tend to dissociate on the same sites more easily to provide more hydrogen atoms, endowing activated N_2 molecules hydrogenating in an alternative way and releasing two-mole NH_3 molecules eventually.

2. Results and Discussion

Figure 1a illustrates the TiO_2(101)-catalyzed mechanochemical N_2 fixation using H_2O as H source. Six potential TMO catalysts, including CuO, Fe_2O_3, TiO_2, Nb_2O_5, ZnO, and Cu_2O, were parallelly evaluated under 25 °C and 1 atm (Figure 1b). The control batch without TMO catalysts gives an NH_4^+ generation rate of 1.310 mg L^{-1} h^{-1}, proving a certain catalytic effect of the milling media themselves.[43] Among all potential TMO catalysts, only TiO_2 and Fe_2O_3 present positive mechanocatalytic activities. The order of NH_4^+ generation rate (unit: mg L^{-1} h^{-1}) is TiO_2 (2.233) > Fe_2O_3 (2.036) > None (1.310) > ZnO (1.267) > Cu_2O (0.849) > Nb_2O_5 (0.408) > CuO (0.245) (Figure 1b). As shown in Figure 1b, the enhanced NH_4^+ generation rate is observed with TiO_2 and Fe_2O_3 as mechanocatalysts, while the NH_4^+ generation rate decreased with the presence of ZnO, Cu_2O, Nb_2O_5, CuO during the mechanochemical reactions. On account of the N_2 and H_2O molecules chemisorbed on transition metal (TM) atoms, the NH_4^+ production per amount of TM-sites should be considered and can be more appropriate to evaluate the performance of these TMO mechanocatalysts. As shown in **Table 1**, the order of NH_4^+ generation rate per amount of TM-site (unit: mg L^{-1} h^{-1} $mol_{TM\text{-}site}^{-1}$) is TiO_2 (35.67) > Fe_2O_3 (32.53) > ZnO (20.64) > Cu_2O (12.17) > Nb_2O_5 (10.85) > CuO (3.90), which is consistent with the order of NH_4^+ generation rate, thus further demonstrates the best mechanocatalytic performance of TiO_2.

To investigate the changes in transition metal oxide before and after mechanochemical reactions, solid powders were collected after each parallel experiment. XRD patterns give the dominant crystal plane of each TMO (Figure 1c). the diffraction peak at 44.5° in all samples arises from the (110) crystal plane of Fe (JCPDS 06–0696), originating from abrasion of mill container and balls.[43] Almost no changes have been observed in their XRD patterns for these transition metal oxides, indicating that the transition metal oxide keeps the same state before and after mechanochemical reactions. The TiO_2 shows a characteristic peak at 25.3° corresponding to the (101) crystal plane of anatase TiO_2 (JCPDS 21–1272), which acts as an active crystal plane for mechanochemical N_2 fixation.

To understand the origin of the significant differences in their mechanocatalytic performance, DFT calculations were performed for these transition metal oxides. It is well known that the adsorption and activation of N_2 on the surface of catalysts is the first step in the N_2 fixation process.[49] The pristine N_2 has an extremely stable triple bond with a bond length of 1.114 Å and only a high energy variation can weaken and prolong N–N bonds. Thus, the N–N bond distance would be a useful criterion to determine the chemisorption and activation behavior of N_2 on the surface of TMO catalysts.[49] Figure 1d and Figure S4 (Supporting Information) show the N–N bond length and adsorption energy (ΔE_1) after N_2 molecules chemisorbing onto the dominant crystal plane of each TMO. The trend of N–N bond length follows Fe_2O_3 (1.140 Å) > Fe (1.137 Å) > TiO_2 (1.129 Å) > ZnO (1.117 Å) > Cu_2O (1.115 Å) > N_2 (1.114 Å) = Nb_2O_5 (1.114 Å) = CuO (1.114 Å). In this dimension of N_2 activation, Fe_2O_3(110) is more effective than TiO_2(101), which is contrary to actual N_2 fixation performance (Figure 1b). Note that hydrogenation is another key process in the ammonia synthesis reaction, and more importantly, in this mechanochemical N_2 fixation process, hydrogen atoms come from the decomposition of chemisorbed H_2O, thus the ability of O–H bond cleavage is another crucial factor.[43] Figure 1e and Figure S4 (Supporting Information) compare the formation energy (ΔE_2) of H-adatom (–H) and OH–adatom (–OH) from H_2O cleavage on the surface of different TMO catalysts. The ΔE_2 on TiO_2(101), Fe(110), and Fe_2O_3(110) surface is −1.15, −0.89, and 0.01 eV, respectively, indicating that –H and –OH adatoms can be generated easily on the TiO_2(101) surface, but hardly on Fe_2O_3(110) surface. Except for TiO_2 and Fe_2O_3, the rest TMOs (CuO, Nb_2O_5, ZnO, and Cu_2O) exhibit little or even negative catalytic activities on neither N_2 activation nor H_2O dissociation. The N–N bond distance of N_2 chemisorbed on the surface of ZnO(101), Cu_2O(111), CuO(111), and Nb_2O_5(001) is 1.117, 1.115, 1.114, and 1.114 Å, respectively,

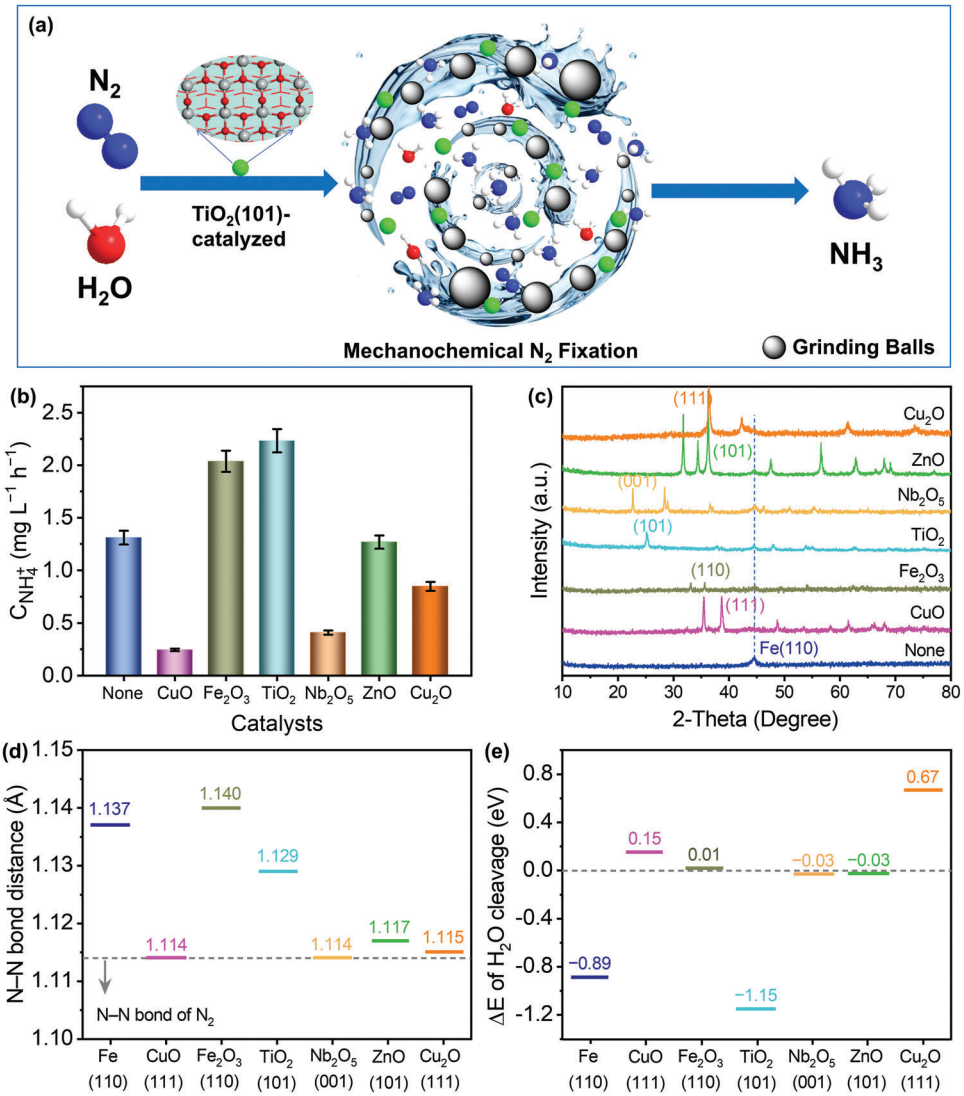

Figure 1. a) Schematic illustration of TiO_2 catalyzed mechanochemical N_2 fixation using H_2O as hydrogen proton sources. b) The ammonia generation rate with different transition metal oxide (TMO) catalysts. The label "None" represents the control experiment without TMO catalysts. The reaction conditions are 280 g ball loading, 600 rpm, and 1 h. c) XRD patterns of solid powders collected after each parallel experiment. d) N—N bond distance of N_2 molecule and e) the cleavage energy of H_2O molecule chemisorbed on Fe(110), CuO(111), Fe_2O_3(110), TiO_2(101), Nb_2O_5(001), ZnO(101), and Cu_2O(111) surfaces.

Table 1. Different types of transition metal oxides (TMOs) and corresponding NH_4^+ production, NH_4^+ production per amount of TMO, and NH_4^+ production per amount of transition metal (TM)-sites.

TMOs	Molar mass of TMOs [g/mol]	Amount of substance [mol]	Amount of TM-sites [mol]	NH_4^+ production [mg L^{-1} h^{-1}]	NH_4^+ production per amount of TMO [mg L^{-1} h^{-1} mol_{cat}^{-1}]	NH_4^+ production per amount of TM-site [mg L^{-1} h^{-1} $mol_{TM\text{-}site}^{-1}$]
TiO_2	79.87	0.0626	0.0626	2.233	35.67	35.67
Fe_2O_3	159.69	0.0313	0.0626	2.036	65.05	32.53
ZnO	81.38	0.0614	0.0614	1.267	20.64	20.64
Cu_2O	143.09	0.0349	0.0698	0.849	24.33	12.17
Nb_2O_5	265.81	0.0188	0.0376	0.408	21.70	10.85
CuO	79.55	0.0629	0.0629	0.245	3.90	3.90

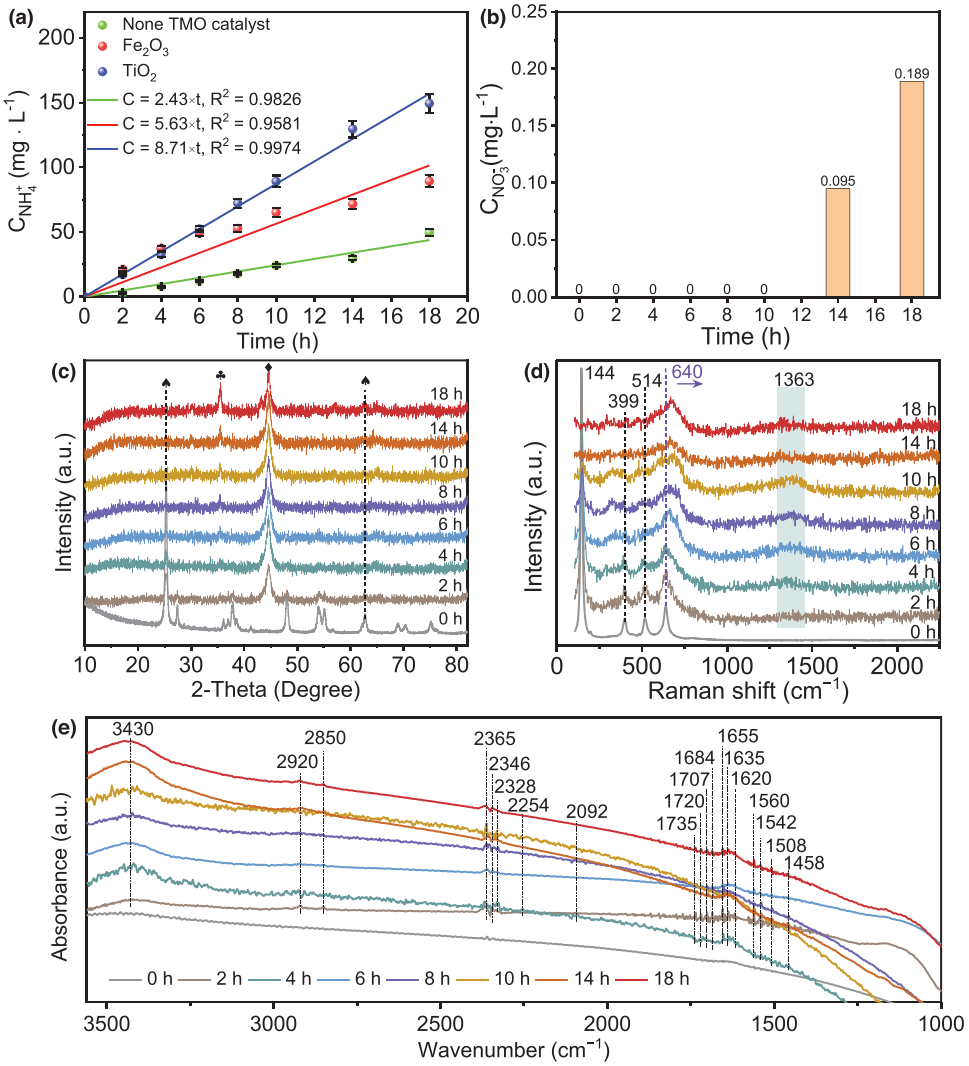

Figure 2. a) NH_4^+ generation rate under optimized experimental parameters (700 g ball loading, 650 rpm) using TiO_2, Fe_2O_3 mechanocatalysts or without TMO catalyst,[43] b) The corresponding NO_3^- generation rate using TiO_2 as mechanocatalyst. The concentration of and NO_3^- is detected by using ion chromatography. c) XRD patterns, d) Raman spectra, and e) FT-IR spectra of solid powders obtained after TiO_2-catalyzed mechanochemical N_2 fixation for 0, 2, 4, 6, 8, 10, 14, and 18 h.

similar to the pristine N_2 (1.114 Å) and much shorter than that of the N_2 chemisorbed on the Fe(110) surface (1.137 Å), illustrating that N_2 can be barely activated on the surface of these four TMOs. Meanwhile, the ΔE_2 of H_2O cleavage on the ZnO(101), Cu_2O(111), CuO(111), and Nb_2O_5(001) surface is –0.03, 0.67, 0.15, and –0.03 eV, which is larger than that on the Fe(110) surface (–0.89 eV), implying that H_2O can be more difficult to dissociate into H-adatoms and OH-adatoms on these TMOs surface. Therefore, a synthetical effect on N_2 activation and H_2O cleavage enables TiO_2(101) and Fe_2O_3(110) remarkable mechanocatalytic activities in this aqueous mechanochemical N_2 fixation.

The time-dependent N_2 fixation using TiO_2 and Fe_2O_3 as mechanocatalysts was evaluated under 25 °C and 1 atm, and the NH_4^+ concentration was measured by ion chromatography (**Figure** 2a) and Nessler's reagent spectrophotometry (Figure S6, Supporting Information). The NH_4^+ production shows a linear relationship with the milling time, so the TMO-catalyzed mechanochemical N_2 fixation is a zero-order reaction. The rate equation is $C(NH_4^+) = 8.71{\times}t$ (mg L^{-1}) for TiO_2 catalyst and $C(NH_4^+) = 5.63{\times}t$ (mg L^{-1}) for Fe_2O_3 as catalyst, verifying that TiO_2 plays an indispensable mechanocatalytic role in this mechanochemical N_2 fixation process, and its catalytic activity is far remarkable than that of Fe_2O_3 or Fe shavings from the milling vessel.[43] The NO_3^- concentration using TiO_2 as mechanocatalyst was also detected by ion chromatography (Figure 2b). No NO_3^- can be detected when the ball milling time is less than 14 h, which may be due to the concentration of NO_3^- is too low. The concentration of NO_3^- for the reaction time of 14 and 18 h is 0.095 and 0.189 mg L^{-1}, and the corresponding NH_4^+ selectivity is 99.924% and 99.868%, respectively. When the ball milling time is more than 14 h, the generated NO_3^- concentration is large enough to be detected. To further evaluate the potential mecanocatalytic N_2 fixation ability of TiO_2 and rule out the effect of Fe contents, comparison experiments without Fe

contents were carried out at room temperature and atmospheric pressure (Figure S7, Supporting Information). Considering that ZrO_2 is less efficient for mechanochemical N_2 fixation than stainless steel[43] but is more robust, 180 g ZrO_2 grinding balls and 100 mL ZrO_2 container were chosen as the ball mill equipment (Figure S7a, Supporting Information) and it would be a fair comparison. As shown in Figure S7b (Supporting Information), from 0 to 6 h, the concentration of NH_4^+ showed a linear relationship with the ball milling time and the NH_4^+ generation rate is 1.55 mg L^{-1} h^{-1}. The mechanochemical N_2 fixation process reached chemical equilibrium after ball milling for 8 h.

To investigate the origin of outstanding mechanocatalytic capability of TiO_2, after the N_2 fixation, the solid powders were collected and characterized accordingly (Figure 2c). The main peak at 25.3°corresponds to the (101) plane of anatase TiO_2, and a minor peak at 27.4° arises from the (110) plane of rutile TiO_2 (JCPDS 87–0920). In Figure 2c, the peak at 35.6° is assigned to (313) plane of Fe_2O_3 (JCPDS 89–5894) and 44.5° comes from (110) crystal plane of Fe. Along with the prolonged ball milling time, the intensity of TiO_2 decreases due to a gradual surface disorder feature, yet the intensity of Fe_2O_3 and Fe increases implying that the wear of the container and balls results in more Fe components and partial Fe may further be oxidized to Fe_2O_3 during the process. According to DFT calculation results, the anatase TiO_2 is more favorable to activating N_2 molecules since the N—N bond length of N_2 on anatase-TiO_2(101) surface (1.129 Å, Figure S4d, Supporting Information) is longer than that on rutile-TiO_2(110) surface (1.114 Å, Figure S4h, Supporting Information). Besides, the anatase-TiO_2(101) surface is more beneficial for H_2O dissociation as well (Figure S4, Supporting Information). Therefore, it is assumed that the anatase phase in TiO_2 (P25) plays a major role in the mechanocatalysis, and the research object in this work is simplified to anatase TiO_2 for further DFT calculations.

Raman scattering is sensitive to crystal defects and the characteristic peaks will shift once the original lattice symmetry is broken or forming a nonstoichiometric crystal.[50,51] Raman spectra were measured for the series of TiO_2 samples before and after mechanochemical reactions for various time. As shown in Figure 2d, the peaks at 144, 399, 514, and 640 cm^{-1} correspond to E_g, B_{1g}, A_{1g}, and E_{1g} modes of anatase TiO_2, respectively,[50–52] and their significantly reduced intensity implies a typical feature of surface disorder.[50] The peak at 640 cm^{-1} blue-shifts when extending the milling time, suggesting the formation of oxygen vacancies (O_v) in the TiO_2 crystal lattice.[50,51] The peak at ≈1363 cm^{-1} arises from Ti—N bonds,[53] indicating the chemisorption of N_2 on the surface of TiO_2.

To further clarify the involvement of TiO_2 in mechanocatalytic ammonia synthesis, the surface-chemisorbed intermediates are investigated by an FT-IR spectrometer (Figure 2e). The existence of stable adsorbates can serve as indicators during mechanochemical N_2 fixation, but the signal of some unstable adsorbates may be hardly captured. In the IR spectra, the broad absorption band at ≈3430 cm^{-1} corresponds to the N—H and/or O—H stretching vibration.[54] The bands at 2920, 1735, 1720, and 1508 cm^{-1} are ascribed to NH_3 molecules, and the band at 2850 cm^{-1} is attributed to NH_4^+ species.[55,56] The peaks at ≈2365 and 2346 cm^{-1} may be originated from the distraction of CO_2 in the air.[43] The peaks at 2328, 2254, and 2092 cm^{-1} are assigned to the N—N stretching vibration of N_2 species.[56,57] Furthermore, vibrational peaks at 1707 and 1560 cm^{-1} come from —NH_2 species while those at 1684 and 1655 cm^{-1} are from —NH species. The bands at ≈1635, 1620, and 1542 cm^{-1} belong to the $\delta_{as}(NH_3)$ of H_2N–NH_3^+.[56] The vibrational peak at 1458 cm^{-1} is ascribed to the —NH_2 scissoring of —N_2H_4 species.[56]

The chemical bonding and surface states of pristine and milled TiO_2 catalysts are investigated by XPS spectroscopy. Except for C, O, and Ti elements in the pristine TiO_2, another two characteristic signals of N and Fe elements emerge in the milled TiO_2 catalysts (**Figure 3a**). In the Ti2p core level (Figure 3b), four sub-peaks of Ti^{3+} $2p_{3/2}$ (456.8 eV), Ti^{4+} $2p_{3/2}$ (459.8 eV), Ti^{3+} $2p_{1/2}$ (462.4 eV), and Ti^{4+} $2p_{1/2}$ (465.4 eV) imply that the pristine TiO_2 itself contains certain oxygen vacancies (O_v) in the presence of Ti^{3+} species.[49,58] For the milled TiO_2, 0.4 eV-shift to lower binding energy and an enlarged content of Ti^{3+} (12.1% of milled TiO_2 versus 10.1% of pristine TiO_2) indicate that more O_v is generated during the ball milling process. Likewise, the peak at 531.8 eV in the O1s core level shifts to a higher binding energy after ball milling for 2 h (Figure 3c), further confirming more O_v in the milled TiO_2. In the high-resolution N1s spectra (Figure 3d), two weak peaks at 401.1 and 402.6 eV are attributed to N_2 physisorption on the surface of pristine TiO_2.[3,59] Two sub-peaks at 400.3 and 401.8 eV in the milled TiO_2 arise from the chemisorption of N_2 molecules.[59] Meanwhile, the sub-peak at 398.8 eV is attributed to the substituted-N by replacing O atoms in the lattice of TiO_2.[60] As shown in Figure S8 (Supporting Information), trivalent Fe that centered at 712.4 and 725.0 eV are also observed in the milled TiO_2.[54,55] The Fe component originates from the wear of stainless steel equipment and is further oxidized during the ball milling process. The electron energy loss spectroscopy (EELS) characterization of Ti-$L_{2,3}$ edge was performed to verify the oxidation state changes in TiO_2 before and after the reactions. According to the literature, the TiO_2 present Ti^{4+} features with two peaks at 458.4 (Ti-L_3) and 463.7 (Ti-L_2) eV, respectively.[49] The Ti $L_{2,3}$ edge of Ti oxides in the EELS spectra shifts to lower energy with decreasing oxidation state (+4, +3, and +2), and the shift of each oxidation state is ≈1.7–2.0 eV.[61] As shown in Figure 3e, the unmilled TiO_2 showed two peaks at 458.1 (Ti-L_3) and 463.4 (Ti-L_2) eV, respectively, shifting 0.3 eV to lower energy compared to the TiO_2 with Ti^{4+} oxidation state in the literature,[49] indicating that the oxidation state of Ti in unmilled TiO_2 is mostly +4 and a small amount is +3. For the TiO_2 milled 2 h, the corresponding two peaks centered at 456.9 and 462.2 eV, showing a shift of 1.2 eV to lower energy for the Ti-L edge in the EELS spectra, implying that the Ti^{3+} content of milled TiO_2 increased after the reaction.

DFT calculations are carried out to further elucidate the catalytic capability of TiO_2 catalysts in mechanochemical N_2 fixation. First, we investigated the possible sites of oxygen vacancies. The mechanical energy generated during ball milling can create fresh reactive surfaces and high active defect sites,[25] so more oxygen vacancies would emerge after ball milling. Figure S9 (Supporting Information) shows two types of oxygen vacancies on the TiO_2(101) surface, namely TiO_2(101)-O_v-1 (bridging oxygen) and TiO_2(101)-O_v-2 (non-bridging oxygen), and their formation energy is 3.93 and 4.16 eV, respectively, so the bridging oxygen vacancies are easier to form on the surface of TiO_2(101). Second, the surface chemisorption and activation of N_2 molecules are of

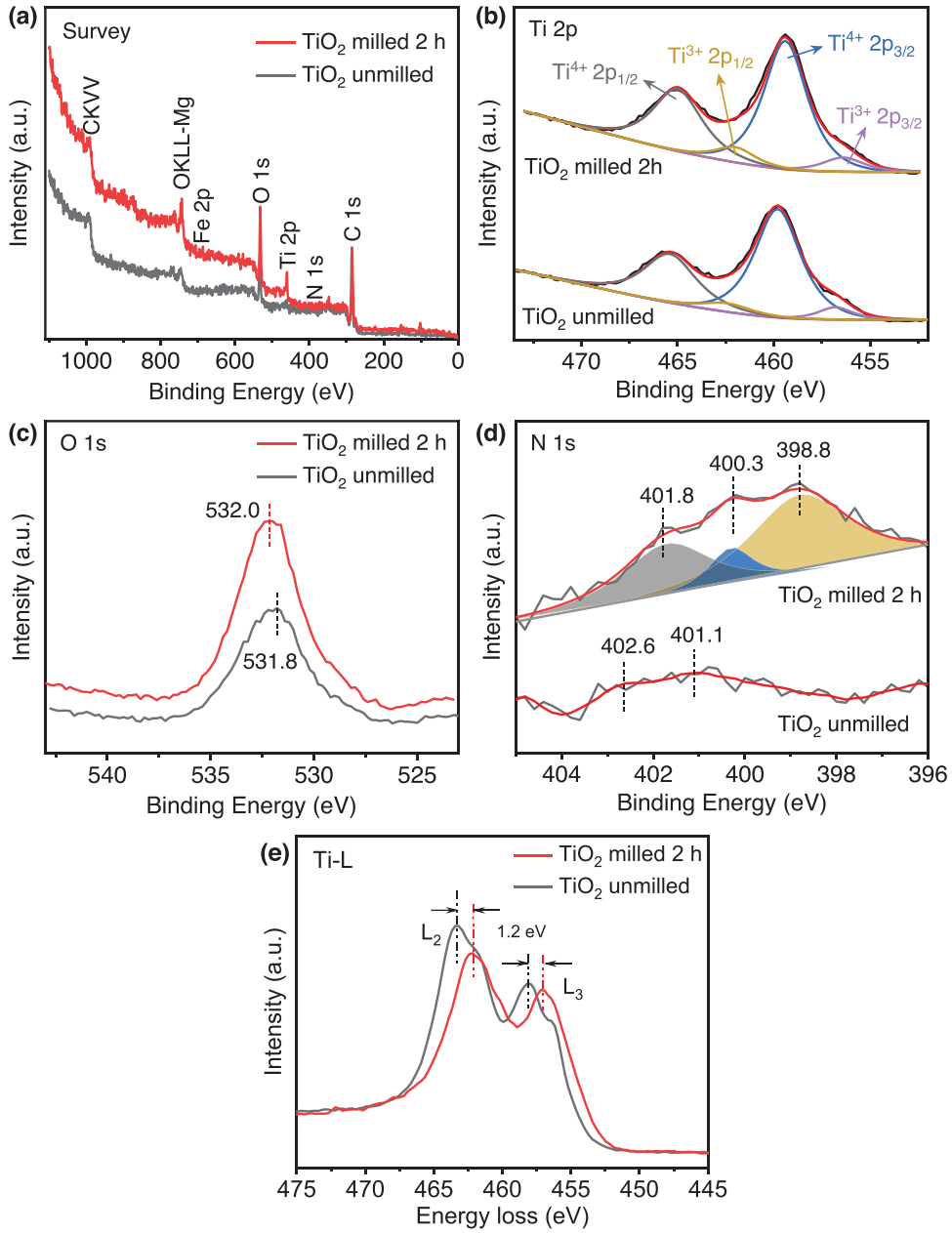

Figure 3. a) XPS spectra and corresponding high-resolution Ti 2p b), O 1s c), and N 1s d) core levels of pristine and milled TiO_2 powders. e) Electron energy loss spectroscopy (EELS) of the Ti-L edge recorded across the pristine TiO_2 and milled TiO_2 powders.

great significance to initialize the mechanochemical N_2 fixation. **Figure** 4a and Table S3 (Supporting Information) present the geometry structure, adsorption energy (ΔE), and N—N bond distance of N_2 chemisorbed on the TiO_2(101) surface under side-on and end-on way. The adsorption energy of N_2 on the O_v sites is −0.92 eV in a side-on way and −0.56 eV in an end-on way, both of which are much higher than that on the Ti sites adjacent to or away from the O_v sites, indicating the favorable N_2 adsorption on the O_v sites. Also, the N—N bond length on the O_v sites (1.192 or 1.141 Å) is much longer than that on the Ti sites (1.115–1.118 Å) and the original N_2 molecule (1.114 Å), suggesting that the N—N bond is weakened and activated effectively.

Figure 4b,c shows the charge density difference of N_2 molecules chemisorbed on TiO_2(101)-O_v-1 in a side-on or end-on way. Electrons transfer between two sideward Ti atoms adjacent to the O_v site and the N_2 molecule through an "acceptance-donation" process, that is, Ti atoms accept lone pair electrons and donate available d-orbital electrons back into the antibonding orbital of π N—N to activate the N_2 molecules.[57] The N—N bond of N_2 chemisorbed in a side-on way (Figure 4b) is weakened and activated more significantly than that in an end-on way (Figure 4c), so N_2 molecules are more favorable to chemisorbing on bridging oxygen vacancies of TiO_2 mechanocatalyst in a side-on way.

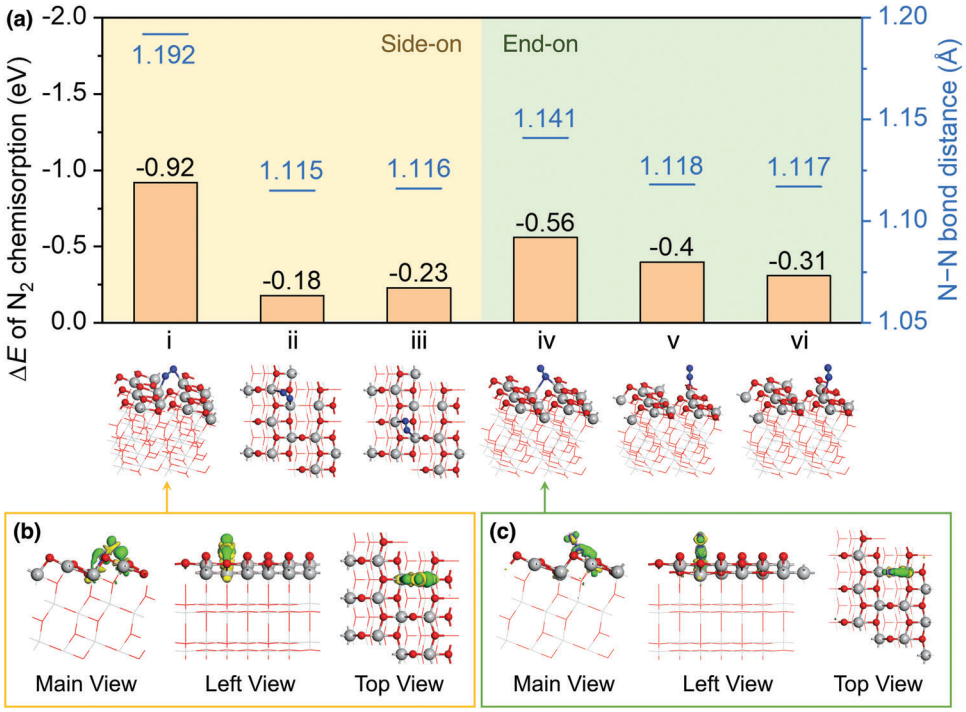

Figure 4. a) The geometry structure of N_2 molecule side-on and end-on chemisorbed on the TiO_2(101)-O_v-1 surface at (i,iv) O_v sites, (ii,v) Ti sites adjacent to O_v, and (iii,vi) Ti sites away from O_v, respectively. Charge density difference of N_2 chemisorbed on the O_v sites in a side-on way b) and end-on way c). The green and yellow iso-surfaces represent the enriched and depleted electron arrangement in space, respectively.

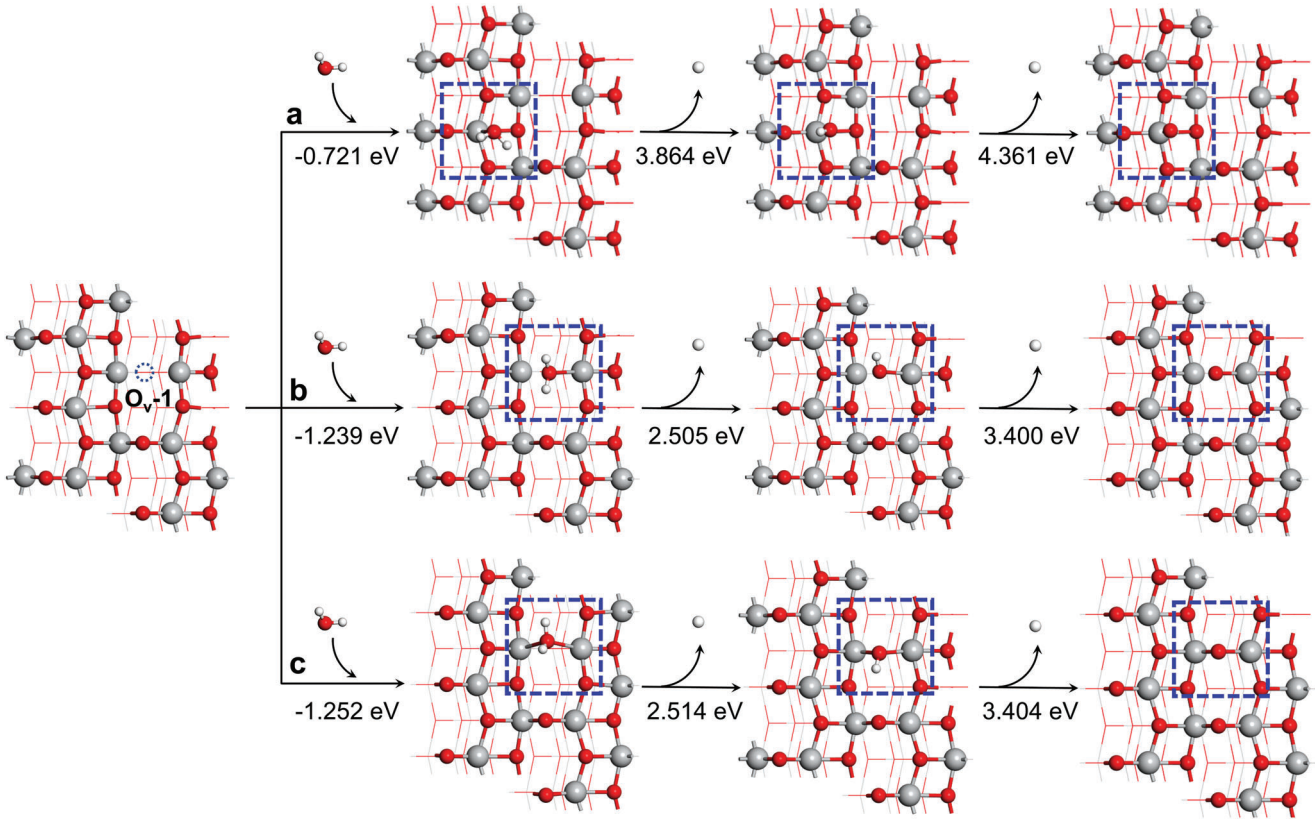

Figure 5. The pathway of H_2O molecules chemisorbed and dissociated on the TiO_2(101)-O_v-1 surface at a) Ti sites away from O_v, b) Ti sites adjacent to O_v, and c) the O_v sites.

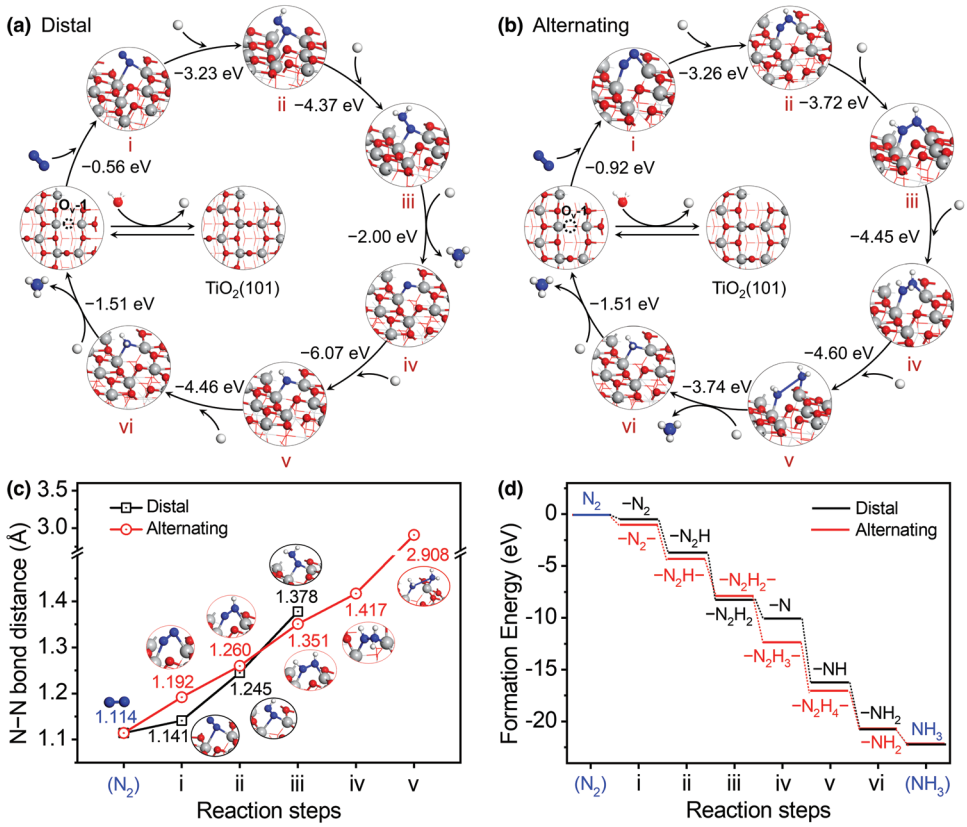

Figure 6. The possible mechanism of mechanochemical N_2 fixation on the TiO_2(101)-O_v-1 surface in a distal pathway a) or an alternating pathway b). The variation of c) N—N bond distance and d) the formation energy at each reaction step.

The chemisorption and dissociation of H_2O is another crucial factor for the involvement of H_2O as the H source in mechanochemical N_2 fixation reaction. Figure S4d (Supporting Information) shows the geometry structure of chemisorbed H_2O molecule, OH-adatom, and H-adatom on the surface of TiO_2(101). The formation energy of OH-adatoms and H-adatoms from H_2O dissociation is initially calculated to be −1.15 eV. **Figure 5** further simulates the process of H_2O molecules dissociating and simultaneously releasing free H . Note that free H are different from H-adatoms due to the need for more energy input. The formation energy of H_2O chemisorbing on the Ti sites away from O_v is −0.721 eV, and that of the O–H bond cleavage to form OH-adatom and then O-adatom is 3.864 and 4.361 eV, respectively (Figure 5a). In comparison, H_2O molecules chemisorbed on the Ti sites adjacent to O_v or on the O_v sites are more feasible in terms of energy variation and the formation energy of two free H is much lower as well (Figure 5b,c). The generated free H are sources for hydrogenating the activated N_2, while the remained O-adatoms may be consumed in the following ways: I) entering the O_v sites (Figure 5c), II) oxidizing the stainless-steel powders to form iron oxides, and III) generating O_2 gases (Figure S10, Supporting Information).

The possible distal or alternating hydrogenation pathways of activated N_2 on the TiO_2(101)-O_v-1 surface are studied (**Figure 6**). Tables S2 and S3 (Supporting Information) show the total energy and optimized geometry structures of various intermediates involved in the reaction. In the distal pathway (Figure 6a), the activated N_2 chemisorbs on the O_v site in an end-on way, and the first-step hydrogenation preferentially occurs on the N atoms farthest from the TiO_2(101)-O_v-1 surface so the terminal N atoms do not directly interact with the catalyst. After releasing the first NH_3 molecule, the remaining lattice N atom is hydrogenated to release the second NH_3 molecule. In the alternating pathway, two N atoms chemisorb on the O_v sites and hydrogenate alternately (Figure 6b), so that all N—N bonds are broken and NH_3 molecules are released from the TiO_2(101)-O_v-1 surface sequentially. Figure 6c shows the N—N bond distance at each elementary reaction step. The O_v sites as side-on chemisorption centers of N_2 molecules increase the N—N bond distance more efficiently, and the N—N bonds are continuously weakened as the hydrogenation process proceeds. In the alternating pathway, the N—N bond distance increases nearly three times before NH_3 release. The change of formation energy (ΔE) at each step is calculated simultaneously (Figure 6d). Once N_2 molecules chemisorb on the bridge-O_v sites, the subsequent hydrogenation with free H atoms either in a distal or alternating pathway is an energy-releasing process. The free H atoms originate from the dissociation of H_2O and its formation energy is 2.51 eV on average (Figure 5). Therefore, the ability of H_2O dissociation to provide H atoms is the rate-determining step in this system. Besides, the direct dissociation of N—N bonds is another potential N_2 fixation route (Figure S11, Supporting Information). Similarly, N_2 molecules first chemisorb on the TiO_2(101)-O_v-1 surface in an end-on or side-on way and then break the N—N bonds to leave

N-adatoms, during which required external energy input is 9.78 and 10.15 eV, respectively. So, the direct dissociation route is not preferred in this process due to a high energy barrier. Therefore, side-on N_2 chemisorption on the bridge-oxygen defect sites of TiO_2(101) surface and H_2O dissociation to generate free H atoms are two key factors in this mechanochemical N_2 fixation under an alternating pathway. Table S4 (Supporting Information) shows the comparison of different ammonia synthesis technologies in recent years.

3. Conclusion

In summary, for the first time, we have demonstrated that TiO_2 can be acted as mechanocatalyst using H_2O as H sources for ammonia synthesis. The mechanocatalytic performance of six transition metal oxides including TiO_2, Fe_2O_3, CuO, Nb_2O_5, ZnO, and Cu_2O was investigated in mechanochemical N_2 fixation. It is found that TiO_2 shows the best mechanocatalytic capability, with the reaction rate constant is 3.6-folds larger than that without catalysts. The DFT calculations indicate that both the chemisorption and activation of N_2 and the H_2O dissociation are two key factors to improve the mechanochemical N_2 fixation performance in $N_2 + H_2O$ system. As for TiO_2, the origin is the mechano-induced bridge-oxygen vacancies in the surface of TiO_2, which are in favor of chemisorption and activation of N_2 molecules in a side-on way, simultaneously facilitated dissociation of H_2O molecules to provide abundant free H atoms, and thus alternative-way hydrogenation to release NH_3. This work not only proposes a mechanocatalytic mechanism driven by defective engineering of TiO_2 but also provides a criterion for catalyst selection to further lower energy barriers in mechanochemical N_2 fixation under mild conditions.

Supporting Information

Supporting Information is available from the Wiley Online Library or from the author.

Acknowledgements

This work was supported by the Natural Science Foundation of Shanghai (20ZR1403300) and the National Natural Science Foundation of China (52002076). The authors appreciate Prof. Shangpeng Gao from Fudan University for his helpful discussions in DFT calculations. The authors also appreciate Dr. Qiaodan Li (Shanghai Huali Integrated Circuit Manufacturing Corporation) for the helpful discussions in DFT calculations.

Conflict of Interest

The authors declare no conflict of interest.

Data Availability Statement

The data that support the findings of this study are available in the supplementary material of this article.

Keywords

Ammonia synthesis, H_2O dissociation, mechanochemistry, N_2 adsorption, TiO_2

Received: October 19, 2023
Revised: November 10, 2023
Published online:

[1] P. Wang, J. Yan, S. Wang, P. Xu, L. Shen, T. Song, *Bioresour. Technol.* **2021**, *340*, 125641.
[2] B.-H. Wang, B. Sun, L. Chen, M.-Q. Cai, S.-F. Yin, *J. Phys. Chem. C* **2021**, *125*, 13212.
[3] G. F. Han, F. Li, Z. W. Chen, C. Coppex, S. J. Kim, H. J. Noh, Z. Fu, Y. Lu, C. V. Singh, S. Siahrostami, Q. Jiang, J. B. Baek, *Nat. Nanotechnol.* **2021**, *16*, 325.
[4] H. Hirakawa, M. Hashimoto, Y. Shiraishi, T. Hirai, *J. Am. Chem. Soc.* **2017**, *139*, 10929.
[5] T. Dai, X. Lang, Z. Wang, Z. Wen, Q. Jiang, *J. Mater. Chem. A* **2021**, *9*, 21219.
[6] H. Tan, Q. Ji, C. Wang, H. Duan, Y. Kong, Y. Wang, S. Feng, L. Lv, F. Hu, W. Zhang, W. Chu, Z. Sun, W. Yan, *Nano Res.* **2021**, *15*, 3010.
[7] Y. Zhang, Q. Zhang, D.-X. Liu, Z. Wen, J.-X. Yao, M.-M. Shi, Y.-F. Zhu, J.-M. Yan, Q. Jiang, *Appl. Catal., B* **2021**, *298*, 120592.
[8] A. J. Medford, M. C. Hatzell, *ACS Catal.* **2017**, *7*, 2624.
[9] B. M. Hoffman, D. Lukoyanov, Z. Y. Yang, D. R. Dean, L. C. Seefeldt, *Chem. Rev.* **2014**, *114*, 4041.
[10] T.-N. Ye, S.-W. Park, Y. Lu, J. Li, M. Sasase, M. Kitano, H. Hosono, *J. Am. Chem. Soc.* **2020**, *142*, 14374.
[11] S. Reichle, M. Felderhoff, F. Schüth, *Angew. Chem., Int. Ed.* **2021**, *60*, 26385.
[12] R. Fu, Z. Pan, X. Mu, J. Li, Q. Zhan, Z. Zhao, X. Mu, L. Li, *J. Mater. Chem. A* **2021**, *9*, 22827.
[13] Z. Zhang, X. Huang, H. Xu, *ACS Appl. Mater. Interfaces* **2021**, *13*, 43632.
[14] C. He, X. Li, D. Qiu, Y. Chen, Y. Lu, X. Cui, *Appl. Surf. Sci.* **2021**, *556*, 149753.
[15] C. He, X. Li, X. Chen, S. Ma, X. Yan, Y. Zhang, S. Zuo, C. Yao, *Appl. Clay Sci.* **2020**, *184*, 105398.
[16] P. Li, Z. Zhou, Q. Wang, M. Guo, S. Chen, J. Low, R. Long, W. Liu, P. Ding, Y. Wu, Y. Xiong, *J. Am. Chem. Soc.* **2020**, *142*, 12430.
[17] N. Zhang, A. Jalil, D. Wu, S. Chen, Y. Liu, C. Gao, W. Ye, Z. Qi, H. Ju, C. Wang, X. Wu, L. Song, J. Zhu, Y. Xiong, *J. Am. Chem. Soc.* **2018**, *140*, 9434.
[18] J. Wang, J. Liang, P. Liu, Z. Yan, L. Cui, L. Yue, L. Zhang, Y. Ren, T. Li, Y. Luo, Q. Liu, X.-E. Zhao, N. Li, B. Tang, Y. Liu, S. Gao, A. M. Asiri, H. Hao, R. Gao, X. Sun, *J. Mater. Chem. A* **2022**, *10*, 2842.
[19] B. Yang, W. Ding, H. Zhang, S. Zhang, *Energy Environ. Sci.* **2021**, *14*, 672.
[20] R. Hawtof, S. Ghosh, E. Guarr, C. Xu, R. M. Sankaran, J. N. Renner, *Sci. Adv.* **2019**, *5*, aat5778.
[21] Y. Gorbanev, E. Vervloessem, A. Nikiforov, A. Bogaerts, *ACS Sustainable Chem. Eng.* **2020**, *8*, 2996.
[22] Y. Bai, J. Lu, H. Bai, Z. Fang, F. Wang, Y. Liu, D. Sun, B. Luo, W. Fan, W. Shi, *Chem. Eng. J.* **2021**, *414*, 128773.
[23] J. Zheng, Y. Lyu, J.-P. Veder, B. Johannessen, R. Wang, R. De Marco, A. Huang, S. P. Jiang, S. Wang, *J. Phys. Chem. C* **2021**, *125*, 23041.
[24] P. M. Chalk, J.-Z. He, M. B. Peoples, D. Chen, *Soil Biol. Biochem.* **2017**, *106*, 36.
[25] A. W. Tricker, K. L. Hebisch, M. Buchmann, Y.-H. Liu, M. Rose, E. Stavitski, A. J. Medford, M. C. Hatzell, C. Sievers, *ACS Energy Lett.* **2020**, *5*, 3362.
[26] C. Bolm, J. G. Hernández, *Angew. Chem., Int. Ed.* **2019**, *58*, 3285.
[27] C. A. Latorre, J. E. Remias, J. D. Moore, H. A. Spikes, D. Dini, J. P. Ewen, *Commun. Chem.* **2021**, *4*, 178.
[28] J.-L. Do, T. Friščić, *ACS Cent. Sci.* **2016**, *3*, 13.
[29] T. Xin, C. C. Cummins, *ACS Cent. Sci.* **2023**, *9*, 1575.

[30] Y. Zhang, Y. Wang, X. Yang, L. Zhao, R. Su, J. Wu, D. Luo, S. Li, P. Chen, M. Yu, Q. Gong, R. Zhu, *Adv. Mater.* **2022**, *34*, 2107420.
[31] Y. Chen, Q. Li, W. Wang, Y. Lu, C. He, D. Qiu, X. Cui, *2D Mater.* **2021**, *8*, 044012.
[32] P. F. M. de Oliveira, R. M. Torresi, F. Emmerling, P. H. C. Camargo, *J. Mater. Chem. A* **2020**, *8*, 16114.
[33] F. Zhai, T. Xin, M. B. Geeson, C. C. Cummins, *ACS Cent. Sci.* **2022**, *8*, 332.
[34] Z. Chen, X. Zhu, J. Yang, J. A. M. Mercer, N. Z. Burns, T. J. Martinez, Y. Xia, *Nat. Chem.* **2020**, *12*, 302.
[35] G. Dayaker, D. Tan, N. Biggins, A. Shelam, J.-L. Do, A. D. Katsenis, T. Friščić, *ChemSusChem* **2020**, *13*, 2966.
[36] H. Zhang, C. E. Diesendruck, *Angew. Chem., Int. Ed.* **2022**, *61*, 202115325.
[37] T.-W. Kwon, B. Song, K. W. Nam, J. F. Stoddart, *J. Am. Chem. Soc.* **2022**, *144*, 12595.
[38] R. Eckert, M. Felderhoff, F. Schüth, *Angew. Chem., Int. Ed.* **2017**, *56*, 2445.
[39] G. Mulas, R. Campesi, S. Garroni, F. Delogu, C. Milanese, *Appl. Surf. Sci.* **2011**, *257*, 8165.
[40] G.-F. Han, P. Zhang, P. Scholzen, H.-J. Noh, M. Yang, D. H. Kweon, J.-P. Jeon, Y. H. Kim, S.-W. Kim, S.-P. Han, A. S. Andreev, G. Lang, K. Ihm, F. Li, J.-B. d'Espinose de Lacaillerie, J.-B. Baek, *Angew. Chem., Int. Ed.* **2022**, *61*, 202117851.
[41] G. Heinicke, K. Meyer, U. Senzky, *Z. Anorg. Allg. Chem.* **1961**, *312*, 180.
[42] Peter, A. Thiejen, G. Heinicke, N. Bock, *Z. Chem.* **1974**, *14*, 76.
[43] C. He, Q. Li, X. Zhang, Y. Lu, D. Qiu, Y. Chen, X. Cui, *ACS Sustainable Chem. Eng.* **2022**, *10*, 746.
[44] Q. Li, L. He, C. Sun, X. Zhang, *J. Phys. Chem. C* **2017**, *121*, 27563.
[45] N. Shan, V. Chikan, P. Pfromm, B. Liu, *J. Phys. Chem. C* **2018**, *122*, 6109.
[46] Y. Abghoui, A. L. Garden, J. G. Howalt, T. Vegge, E. Skúlason, *ACS Catal.* **2016**, *6*, 635.
[47] Y. Abghoui, E. Skúlason, *Catal. Today* **2017**, *286*, 69.
[48] B. Hu, M. Hu, L. Seefeldt, T. L. Liu, *ACS Energy Lett.* **2019**, *4*, 1053.
[49] N. Cao, Z. Chen, K. Zang, J. Xu, J. Zhong, J. Luo, X. Xu, G. Zheng, *Nat. Commun.* **2019**, *10*, 2877.
[50] C. Li, M. Gu, M. Gao, K. Liu, X. Zhao, N. Cao, J. Feng, Y. Ren, T. Wei, M. Zhang, *J. Colloid Interface Sci.* **2022**, *609*, 341.
[51] J. Wang, W. Lin, Y. Ran, J. Cui, L. Wang, X. Yu, Y. Zhang, *J. Phys. Chem. C* **2020**, *124*, 1253.
[52] X. Bi, G. Du, A. Kalam, D. Sun, Y. Yu, Q. Su, B. Xu, A. G. Al-Sehemi, *Chem. Eng. Sci.* **2021**, *234*, 116440.
[53] S. Zhu, L. Xiao, M. B. Cortie, *Vib. Spectrosc.* **2016**, *85*, 146.
[54] C. Yao, R. Wang, Z. Wang, H. Lei, X. Dong, C. He, *J. Mater. Chem. A* **2019**, *7*, 27547.
[55] Y. Bo, H. Wang, Y. Lin, T. Yang, R. Ye, Y. Li, C. Hu, P. Du, Y. Hu, Z. Liu, R. Long, C. Gao, B. Ye, L. Song, X. Wu, Y. Xiong, *Angew. Chem., Int. Ed.* **2021**, *60*, 16085.
[56] L. R. Winter, B. Ashford, J. Hong, A. B. Murphy, J. G. Chen, *ACS Catal.* **2020**, *10*, 14763.
[57] Y. Zhang, X. Chen, S. Zhang, L. Yin, Y. Yang, *Chem. Eng. J.* **2020**, *401*, 126033.
[58] Q.-Y. Liu, H.-D. Wang, R. Tang, Q. Cheng, Y.-J. Yuan, *ACS Appl. Nano Mater.* **2021**, *4*, 8674.
[59] R. Asahi, T. Morikawa, T. Ohwaki, K. Aoki, Y. Taga, *Science* **2001**, *293*, 269.
[60] Z. Ding, M. Sun, W. Liu, W. Sun, X. Meng, Y. Zheng, *Sep. Purif. Technol.* **2021**, *276*, 119287.
[61] E. Stoyanov, F. Langenhorst, G. Steinle-Neumann, *Am. Mineral.* **2007**, *92*, 577.